Structure

Article

The CC1-FHA Tandem as a Central Hub for Controlling the Dimerization and Activation of Kinesin-3 KIF1A

Lin Huo,[1,2,5] Yang Yue,[1,3,5] Jinqi Ren,[1] Jiang Yu,[2,6] Junlin Liu,[1] Yong Yu,[1] Fei Ye,[2] Tao Xu,[1,3,*] Mingjie Zhang,[2,4,*] and Wei Feng[1,*]

[1]National Laboratory of Biomacromolecules, Institute of Biophysics, Chinese Academy of Sciences, 15 Datun Road, Beijing 100101, China
[2]Division of Life Sciences, State Key Laboratory of Molecular Neuroscience, Hong Kong University of Science and Technology, Clear Water Bay, Kowloon, Hong Kong, China
[3]College of Life Science and Technology, Huazhong University of Science and Technology, Wuhan 430074, China
[4]Center of Systems Biology and Human Health, Hong Kong University of Science and Technology, Clear Water Bay, Kowloon, Hong Kong, China
[5]These authors contributed equally to this work
[6]Present address: School of Physics, University of New South Wales, Sydney NSW 2052, Australia
*Correspondence: xutao@ibp.ac.cn (T.X.), mzhang@ust.hk (M.Z.), wfeng@ibp.ac.cn (W.F.)
http://dx.doi.org/10.1016/j.str.2012.07.002

SUMMARY

Kinesin-3 KIF1A plays prominent roles in axonal transport and synaptogenesis. KIF1A adopts a monomeric form in vitro but acts as a processive dimer in vivo. The mechanism underlying the motor dimerization is poorly understood. Here, we find that the CC1-FHA tandem of KIF1A exists as a stable dimer. The structure of CC1-FHA reveals that the linker between CC1 and FHA unexpectedly forms a β-finger hairpin, which integrates CC1 with FHA assembling a CC1-FHA homodimer. More importantly, dissociation of the CC1-FHA dimer unleashes CC1 and the β-finger, which are both essential for the motor inhibition. Thus, dimerization of the CC1-FHA tandem not only promotes the KIF1A dimer formation but also may trigger the motor activity via sequestering the CC1/β-finger region. The CC1-FHA tandem likely functions as a hub for controlling the dimerization and activation of KIF1A, which may represent a new paradigm for the kinesin regulation shared by other kinesin-3 motors.

INTRODUCTION

Kinesin family proteins (KIFs) are microtubule-dependent molecular motors responsible for long-distance intracellular transport of membrane vesicles/organelles, protein complexes and mRNAs in polarized cells (Hirokawa et al., 2009; Vale, 2003). A total of 45 mammalian KIF genes are known to date, and they are classified into 14 subfamilies (kinesin-1 to kinesin-14) (Lawrence et al., 2004). Kinesin-3 KIF1A was originally identified in a systematic screening of murine brain cDNAs required for neuronal transport (Aizawa et al., 1992). Subsequent studies revealed that KIF1A is chiefly responsible for fast anterograde transport of synaptic vesicle (SV) precursors in axons (Okada

et al., 1995), and deficiency of this motor resulted in dramatic decreases of SV densities and accumulations of small vesicles in the soma (Yonekawa et al., 1998). Recently, KIF1A has been found to participate in the regulation of interkinetic nuclear migration during embryonic brain development (Tsai et al., 2010). Coordinated activation of UNC-104 (KIF1A homolog in *Caenorhabditis elegans*) and another type of microtubule-dependent motor dynein is also essential for patterning newly formed synapses (Park et al., 2011). Thus, KIF1A/UNC-104 may be fundamental for both neuronal development and synaptogenesis. Given aforementioned functions of KIF1A/UNC-104 in neurons, it is not surprising that mutations of this motor are coupled with a number of human neuronal disorders, such as "hereditary sensory and autonomic neuropathy type II" and "hereditary spastic paraparesis" (Erlich et al., 2011; Rivière et al., 2011).

In the conventional kinesin, kinesin-1 KIF5A, the motor domain (MD) and neck coil (NC) are immediately followed by a central stalk region (stalk CC1) (Figure 1A), which is able to form a coiled-coil dimer for assembling the "two-headed" kinesin-1 motors (Vale, 2003; Verhey et al., 2011). With the two motor heads, kinesin-1 motors employ the "hand-over-hand" mechanism for the processive movement on microtubule tracks (Gennerich and Vale, 2009; Woehlke and Schliwa, 2000; Yildiz and Selvin, 2005). In contrast, in kinesin-3 KIF1A, the central region immediately following MD-NC is predicted to be composed of a number of short noncontinuous coiled-coil domains (CC1 to CC3) and a well-defined FHA domain in the middle (Figure 1A). Possibly due to this sharp variation, kinesin-3 KIF1A was initially found to exist as a globular monomer in vitro and denoted as an unconventional "single-headed" kinesin (Okada et al., 1995). However, recent studies of KIF1A have shown that the motor can be detected as a processive dimer in vivo (Hammond et al., 2009). Moreover, another kinesin-3 motor from *Drosophila*, kinesin-73, has been found to adopt a dimeric form in vivo as well (Huckaba et al., 2011). Thus, kinesin-3 motors may not be "single-headed" kinesins but most likely function as "two-headed" processive dimers for cargo transport analogous to kinesin-1 motors. Further supporting this hypothesis, a series
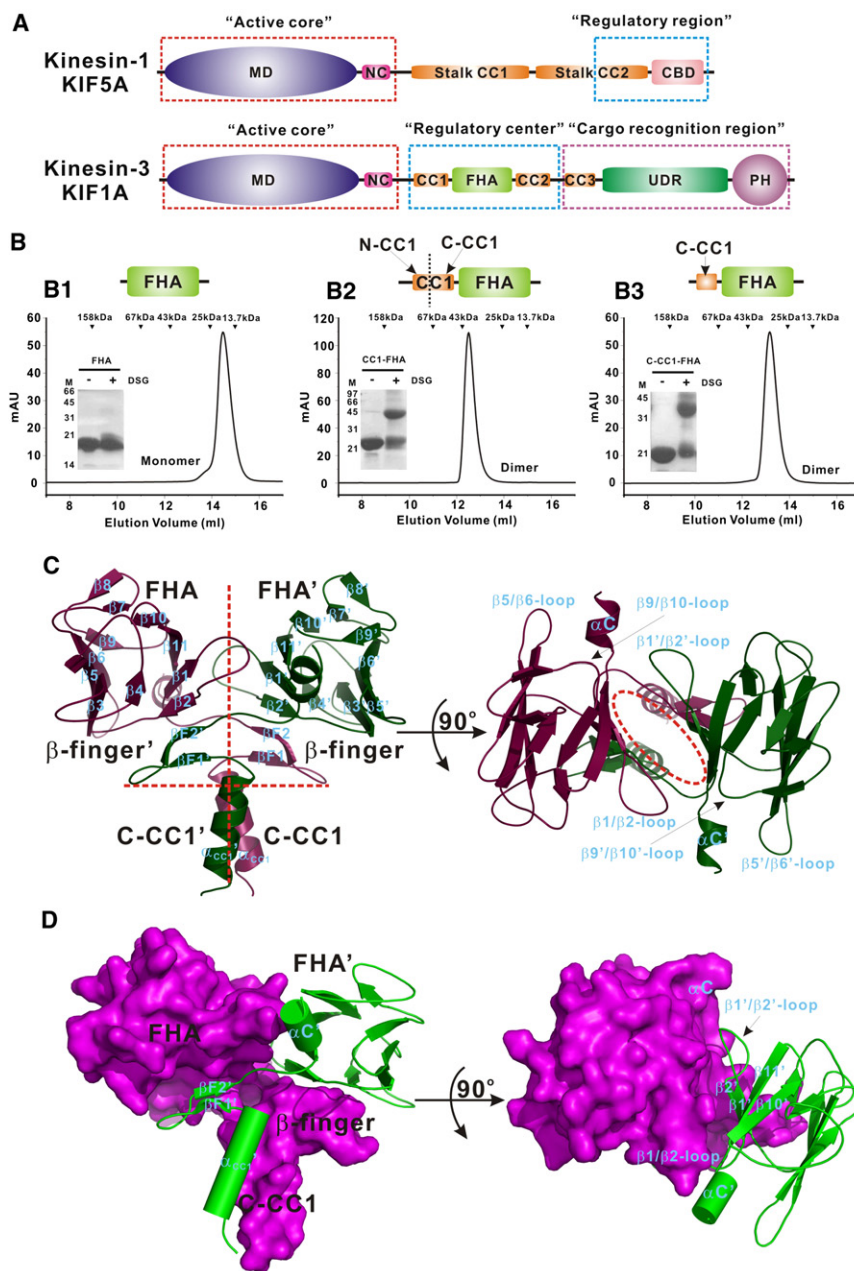
Figure 1. Structure of the C-CC1-FHA Dimer

(A) Domain organization of KIF1A and KIF5A. KIF1A is composed of an N-terminal motor domain (MD) followed by a neck coil (NC), a CC1-FHA-CC2-CC3 in the middle, an undefined region (UDR), and an extreme C-terminal PH domain. The MD and NC forms the active core, the CC1-FHA-CC2 acts as the regulatory center, and the CC3-UDR-PH functions as the cargo recognition region. KIF5A is composed of an N-terminal MD-NC active core, two stalk coiled-coil domains (CC1 and CC2) in the middle, and a C-terminal cargo-binding domain (CBD).

(B) Biochemical characterization of the KIF1A fragments immediately following MD-NC. Analytic gel-filtration analysis assaying the dimerization status of purified the FHA domain (B1), CC1-FHA (B2), and C-CC1-FHA (B3). The elution volumes for MW markers are indicated at the top of each fragment elution profile. The dimerization status of each fragment was further probed by the Lys-mediated chemical crosslinking (shown as the insert of each panel). The data revealed that the C-terminal half of CC1 and the FHA domain together form the minimal dimerization region of the CC1-FHA tandem.

(C) Ribbon diagram of the C-CC1-FHA dimer structure. Two subunits of the C-CC1-FHA dimer are colored in purple and green, respectively. The secondary structures (from β1 to β11) of the FHA domain are labeled following the scheme for the canonical FHA domain. The β-finger (βF1 and βF2) and the C-CC1 helix are also labeled. Notably, the last helices (αC) of two FHA domains contact with the β1/β2 loop, the β5/β6 loop, and the β9/β10 loop.

(D) A combined surface and ribbon representation of the C-CC1-FHA dimer structure. One of the two subunits of the C-CC1-FHA dimer is in the surface representation (colored in purple), and the other is in the ribbon representation (colored in green). The figure clearly shows the extensive contacts between the two subunits of the C-CC1-FHA dimer.

of biochemical/biophysical studies of KIF1A/UNC-104 showed that, similar to kinesin-1 motors, NC of the motor is capable of mediating the motor dimerization (Figure 1A) (Hammond et al., 2009; Rashid et al., 2005; Tomishige et al., 2002). However, the NC dimer seems to be not very stable, as the motors often pause during the movement possibly due to the temporary unwinding of the NC dimer (Rashid et al., 2005; Tomishige et al., 2002). Given that kinesin-1 motors often possess multiple dimeric regions (Figure 1A), it remains to be determined whether regions other than NC may also contribute to the formation of the KIF1A/UNC-104 dimer.

As a characteristic of KIF1A/UNC-104, the central region of the motor including the CC1-FHA-CC2 domains has been found to

be involved in the direct control of the motor activity (Figure 1A). CC1 was reported to sequester NC forming an intramolecular NC/CC1-helix bundle, which prevents the intermolecular NC dimer formation and thus inhibits the motor activity (Al-Bassam et al., 2003). Furthermore, CC2 was found to adopt a folded-back conformation through the interaction with the neighboring FHA domain (Lee et al., 2004). Although neither the FHA domain nor CC2 contacts with MD-NC, the intramolecular interaction between these two domains also leads to the motor inactivation. Therefore, the central CC1-FHA-CC2 domains may function as a negative "regulatory center" in the motor (Figure 1A). However, the molecular mechanism underlying the central region-mediated regulation is not well understood.

In this study, we characterized both CC1 and the FHA domain in the central region of KIF1A and found that only the covalently

linked CC1-FHA tandem forms a stable dimer in solution. The crystal structure of the CC1-FHA tandem uncovered that the linker between CC1 and the FHA domain unexpectedly forms a β-hairpin structure (referred to as β-finger), which assembles both CC1 and the FHA domain thus forming a CC1-FHA homodimer. We further demonstrated that dissociation of the CC1-FHA dimer unleashes CC1 and the β-finger, which are both essential for the motor inhibition. Hence, the CC1-FHA tandem-mediated dimerization not only promotes the formation of the KIF1A dimer but also may prevent the CC1/β-finger-mediated inhibition. The CC1-FHA tandem likely acts as a regulatory hub for controlling the dimerization and activation of KIF1A.

RESULTS

The CC1-FHA Tandem of KIF1A Forms a Stable Dimer in Solution

To investigate whether the central region immediately following MD-NC bears the dimerization capacity, we set out to purify and biochemically characterize the KIF1A fragments centered on the FHA domain (Figure 1A), as this domain is a well-defined protein-protein interaction module (Liang and Van Doren, 2008; Mahajan et al., 2008). Consistent with the current knowledge of the FHA domain (e.g., not specific for the dimerization of proteins), the FHA domain of KIF1A alone stays as a monomer in solution based on both the analytical gel-filtration analysis and the chemical crosslinking assay (Figure 1B1). The N-terminal extension of the FHA domain to CC1 unexpectedly resulted in a stable CC1-FHA dimer (Figure 1B2). To further delineate the role of CC1 for the CC1-FHA dimer formation, we deleted the N-terminal half of CC1. Surprisingly, the remaining fragment (C-CC1-FHA) retains as a dimer in solution (Figure 1B3), suggesting that formation of the CC1-FHA dimer only requires the C-terminal half of CC1 (see below for details). Therefore, the FHA domain of KIF1A together with its N-terminal extension containing the C-terminal half of CC1 forms a stable dimer in solution.

The Overall Structure of the C-CC1-FHA Dimer

The finding of the CC1-FHA dimer supports the view that the central region immediately following MD-NC is capable of promoting the KIF1A dimer formation, which is functionally similar to the central coiled-coil stalk of kinesin-1 (Figure 1A). To uncover the molecular basis governing the CC1-FHA dimer formation, we first determined the crystal structure of C-CC1-FHA to 1.9 Å resolution (Figure 1C and Table 1), as this KIF1A fragment is the minimum region demonstrated above to be required for the formation of the CC1-FHA dimer (Figure 1B). In the crystal structure, C-CC1-FHA forms a symmetric dimer with a "Y" shape (Figure 1C). The two FHA domains are partially separated resembling the two arms, while the two C-CC1s pack with each other forming a short coiled coil as the base. As expected, the FHA domain adopts a classical FHA domain fold with eleven strands (from β1 to β11) forming a two-layered β sandwich and C-CC1 forms a short α-helical structure (α_{CC1}) (Figure 1C). The most unexpected feature in the C-CC1-FHA dimer is that the covalent linker between C-CC1 and the FHA domain is well folded and forms a β-finger structure containing two antiparallel β strands, βF1 and βF2 (Figure 1C). More significantly, the β-finger of one molecule in the C-CC1-FHA dimer crosses over to augment one of the two β sheets of the FHA domain (the β2/β1/β11/β10 sheet) in the other molecule (Figures 1C and 1D). Thus, the C-CC1-FHA dimer of KIF1A is a domain-swapped homodimer assembled by the β-finger structure.

The β-Finger Integrates the C-CC1-FHA Dimer Structure

In the C-CC1-FHA structure, the dimer interface, which occupies ~2,100 Å^2, is formed by several parts, namely the small C-CC1 coiled coil, the short antiparallel β-finger, and the β1/β2 region of the FHA domain (Figure 1C). The formation of the C-CC1 coiled coil is essentially contributed by hydrophobic packing and electrostatic interactions (Figures 2A and 2B). As one of the key components to assemble the homodimer, the β-finger not only forms hydrophobic contacts with the C-CC1 coiled coil, but also physically expands the β sandwich core of the FHA domain (Figures 2A–2C). The residues V474, M476, T482, and V485 from one side of the β-finger make hydrophobic contacts with the residues L468, L469, and M472 from C-CC1 (Figure 2B), while the residues A475, L483, and F486 from the other side of the β-finger pack with the residues Y509 from β2 and C506 from the β1/β2-loop of the FHA domain (Figure 2C).

Table 1. Data Collection and Refinement Statistics of KIF1A CC1-FHA and C-CC1-FHA

Diffraction Data	CC1-FHA	C-CC1-FHA
Space group	$P2_12_12_1$	$P1$
Unit cell (Å)	a = 83.943	a = 42.945
	b = 87.855	b = 57.844
	c = 101.694	c = 110.394
	α = β = γ = 90°	α = 89.978°, β = 89.957°, γ = 90.627°
Resolution (Å)	50.0–2.51 (2.54–2.51)	50.00–1.90 (1.97–1.90)
Observed reflections	66,936	82,040
Unique reflections	25,983	21,035
Rmerge[a] (%)	10.3 (54.4)	7.1 (42.3)
I/σ	14.8 (1.6)	21.28 (3.55)
Average redundancy	2.6 (2.4)	3.93 (4.00)
Completeness (%)	97.6 (97.7)	97.2 (96.5)
Refinement		
R_{work}[b]/R_{free}[c]	25.2/28.2	18.7/23.1
Mean B factors (Å^2)	39.2	44.2
Bond length[d] (Å)	0.010	0.007
Bond angles (°)	1.267	1.109
Ramachandran plot (residues, %)		
Most favored	92.0	93.6
Additionally allowed	8.0	6.4

The values in parentheses refer to the highest resolution shell.
[a]$R_{merge} = \Sigma h\Sigma i \mid I_i (h) \mid \Sigma h\Sigma i (Ih)$, where (Ih) is the mean intensity of the i observations of reflection h.
[b]$R_{factor} = \Sigma h \mid |F_{obs}| - |F_{calc}| \mid /\Sigma |F_{obs}|$, where $|F_{obs}|$ and $|F_{calc}|$ are the observed and calculated structure factor amplitudes, respectively. Summation includes all reflections used in the refinement.
[c]$R_{free} = \Sigma \mid |F_{obs}| - |F_{calc}| \mid /\Sigma |F_{obs}|$, evaluated for a randomly chosen subset of 5% of the diffraction data not included in the refinement.
[d]Rmsd from ideal values.

Figure 2. Interface of the C-CC1-FHA Dimer

(A) Structural-based sequence alignment of KIF1A CC1-FHA from different species. The identical residues are colored in red, and the highly conserved residues are colored in green. The residue numbers and the secondary structures are marked on the top, and the hydrophobic residues responsible for the FHA domain core packing and the dimer interface formation are highlighted with orange dots and yellow triangles, respectively, at the bottom. The charged residues responsible for the dimer interface formation are highlighted with blue triangles.

(B–E) Structure-based analysis of the C-CC1-FHA dimer interface. A combined ribbon and stick-model representation showing the packing interface between CC1 and the β-finger (B), between the β-finger and the FHA domain (C), between two FHA domains (D), and between the β1/β2-loop and αC (E). In addition to extensive hydrophobic packing, electrostatic interactions are complementary for the dimer interface formation. In this drawing, two subunits of the C-CC1-FHA dimer are colored in purple and green, respectively, and the side chains of the residues involved in hydrophobic packing and electrostatic interactions are drawn in explicit atomic model. The clusters of the contact residues in the dimer interface are marked with dashed circles.

hydrophobic contacts, which drive the central β sandwich formation (Figures 1C, 2D, and 2E). Additionally, the β1/β2-loop of one FHA domain further contacts with the C-terminal helix (αC), β10, and β11 of the other FHA domain in the dimer. The residues P501 and L502 from the β1/β2-loop pack with the residues P597 and A600 from αC (Figures 2A and 2E). The negatively charged residues (i.e., E499 and D500) from the β1/β2-loop form electrostatic interactions with the positively charged residues located in β10, β11, and αC (i.e., R583, R593, and R604), which may further stabilize the domain-swapped homodimer (Figures 1C and 2E). Structure-based sequence alignment of C-CC1-FHA demonstrated

Furthermore, the βF1/βF2-loop of the β-finger forms additional electrostatic interactions with the β3/β4-loop of the FHA domain, which may stabilize the packing between the β-finger and the FHA domain (Figure 2C). Thus, the β-finger structurally integrates C-CC1 with the FHA domain forming a domain-swapped C-CC1-FHA dimer, and a central β sandwich is thereby formed by βF1, βF2, β1, and β2 in the dimer structure with one end capped by the short C-CC1 coiled coil (Figure 1C).

The inter-FHA domain interface in the C-CC1-FHA dimer is largely formed by a number of hydrophobic residues from the β1/β2 region of the FHA domain. The residues P488 from the βF2/β1-loop, H493, V495, and L497 from β1, L507, L508, and Y510 from β2, and M503 from the β1/β2-loop form a cluster of

that the residues in C-CC1, the β-finger as well as those in the β1/β2 region of the FHA domain responsible for the dimer interface packing are highly conserved (Figure 2A), suggesting that the C-CC1-FHA dimer and the dimer packing interface are the general features of KIF1A.

The Crystal Structure of the CC1-FHA Tandem

Although the C-CC1-FHA structure essentially revealed the dimeric feature of the CC1-FHA tandem, the N-terminal half of CC1 was removed. To figure out the conformational property of the overall CC1, we next determined the crystal structure of the CC1-FHA tandem to 2.3 Å resolution (Figure 3A and Table 1). Unexpectedly, in contrast to the symmetric C-CC1-FHA dimer

Structure

The CC1-FHA Tandem As a Motor Regulation Hub
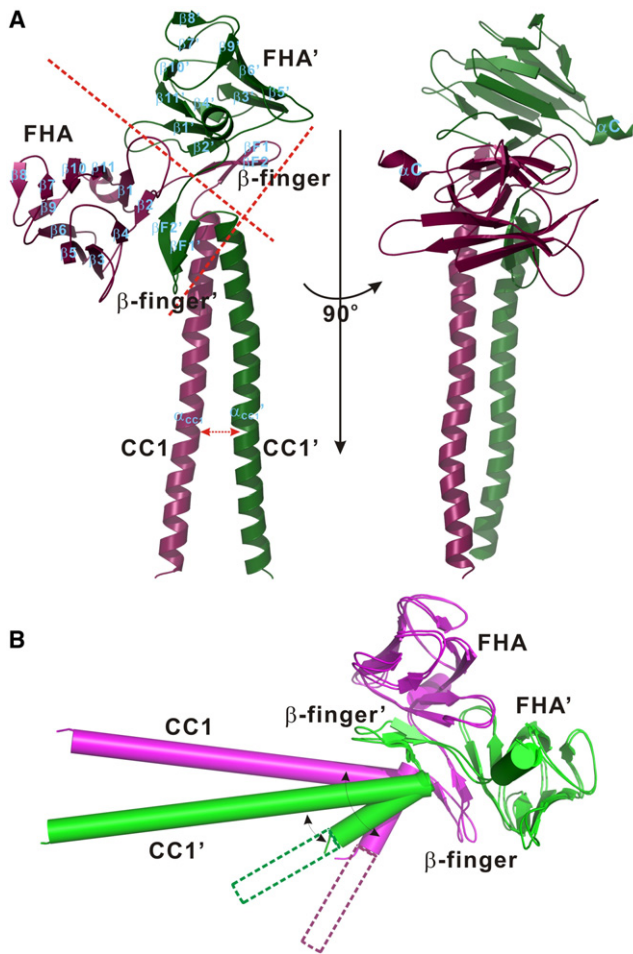
Figure 3. Overall Structure of the CC1-FHA Dimer

(A) Ribbon diagram of the CC1-FHA dimer structure. Two subunits of the CC1-FHA dimer are colored in purple and green, respectively. The secondary structures of the FHA domain, the β-finger, and the CC1 helix are labeled as Figure 1C. Distinctively, the CC1-FHA tandem forms an asymmetric dimer, and the N-terminal halves of the two CC1 helices are largely separated with little contacts.

(B) Comparison of the structure of the CC1-FHA dimer with that of the C-CC1-FHA dimer. Superimposition of the two dimer structures revealed that the FHA domain and the β-finger are essentially the same, but CC1 is quite different in terms of the helix orientation with respect to the β-finger/FHA region. See also Figures S1 and S2.

(Figure 1C), the CC1-FHA tandem forms an asymmetric dimer with a kite-like shape (Figure 3A). The two FHA domains form the two halves of the kite head, and the two CC1 helices act as the tail of the kite (Figure 3A). The "kite tail" formed by the two CC1 helices is tilted as if the kite is flying under the influence of the wind. In the CC1-FHA dimer, CC1 forms an elongated single helix (α_{CC1}). The N-terminal halves of the two CC1 helices are parallel to each other with little interhelical contacts, while the C-terminal half of CC1 forms a short parallel coiled coil similar to that in the C-CC1-FHA dimer (Figures 3A and 4A). Several hydrophobic residues in the short coiled coil (L468, L469, and M472) make contacts with a number of hydrophobic residues from only one of the two β-fingers (e.g., V474, M476, and

V485), thus causing the formation of the asymmetric CC1-FHA dimer (Figures 3A and 4A).

The C-CC1-FHA structure is symmetric (Figure 1C), whereas the CC1-FHA structure is asymmetric (Figure 3A). To explore whether the symmetric or the asymmetric assembling feature is the intrinsic property of the CC1-FHA tandem, we next checked the intermolecular packings of the CC1-FHA structure in the crystal. Analysis of the crystal packing of CC1-FHA revealed that the two N-terminal halves of CC1 from one molecule pack in antiparallel with the same regions of CC1 from another molecule, forming a four helix bundle (crystal packing site I in Figure S1 available online). Additionally, one side of the FHA dimer contacts with another FHA dimer in the asymmetric unit of the crystal, which would "push" the CC1 helix toward the noncontacting FHA domain (crystal packing site II in Figure S1). Therefore, the crystal packing causes the tilting of CC1 relative to the FHA domain, and the asymmetric structural feature is unlikely to be an intrinsic property of the CC1-FHA dimer (Figure 3B).

Further comparison of the structure of the CC1-FHA dimer with that of the C-CC1-FHA dimer showed that both the FHA domain and the β-finger are essentially the same (Figure 3B). Therefore, the dimer interface in the CC1-FHA dimer (buried with ~2,400 Å^2) should be largely comparable to that in the C-CC1-FHA dimer, which is mediated by the hydrophobic residues from the C-terminal half of CC1, the β-finger, and β1/β2 of the FHA domain (Figures 2 and 3). To further evaluate the roles of these hydrophobic residues in the CC1-FHA dimer formation, we made a series of mutations in the CC1-FHA tandem, either with the deletion of the β-finger ([474-486]Δ) or by the substitution of the hydrophobic residues with hydrophilic ones in the dimer interface (L469Q/M472Q, V474N, V485N, V495N, and L508Q/Y510Q), and assayed the dimerization status of these mutants subsequently. Consistent with the above structure-based analysis, most of these CC1-FHA mutants lost the capacity to form a stable dimer in solution (Figure S2).

Both CC1 and the β-Finger Are Essential for the Inhibition of the Motor Activity

The crystal structure of the CC1-FHA tandem revealed that CC1 does not form a coiled-coil dimer (Figure S1 and Figure 4A). Further supporting this, we biochemically characterized the longer CC1-β-finger fragment (that ensures the intactness of the whole CC1 segment) in vitro, and found that the CC1-β-finger fragment stays as a monomer in solution based on both the gel-filtration analysis and the ultracentrifugation assay (Figure 4B). Instead, CC1 adopts an amphipathic helical structure, i.e., one side of the CC1 helix is hydrophilic and enriched with charged residues, while the other side is much hydrophobic (Figure S3). Analysis of the crystal packing of the CC1-FHA structure showed that CC1 tends to form a bundle-like structure mediated by the hydrophobic side of the domain (Figure S1). Therefore, the hydrophobic side of CC1 may provide a potential binding site, and the amphipathic property of CC1 may allow the domain to bind to potential substrates.

Consistent with the features of CC1, it has been reported that CC1 is able to sequester NC in parallel forming a bundle-like structure for the motor inhibition (Al-Bassam et al., 2003; Hammond et al., 2009). In their studies, the KIF1A fragment in the inhibited conformation was defined from the site immediately
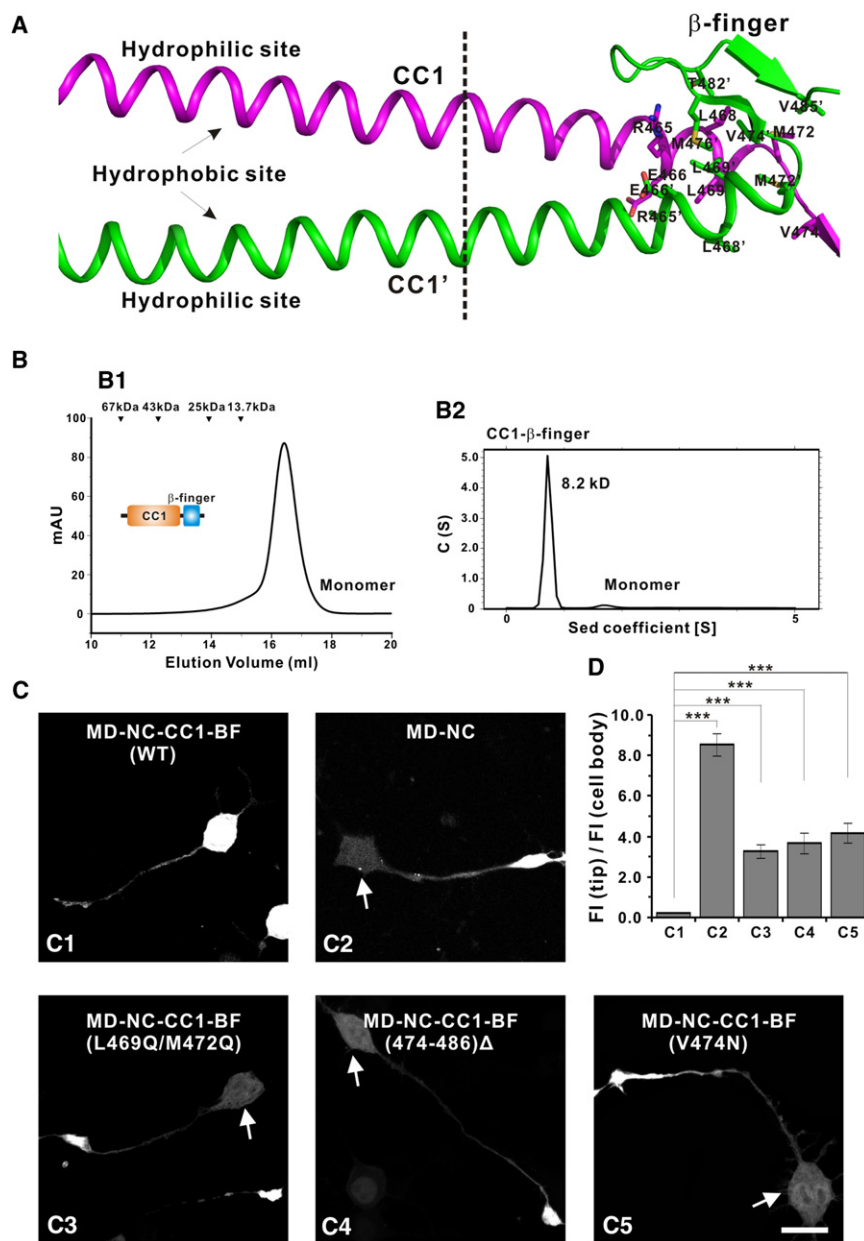
Figure 4. CC1 and the β-Finger Are Both Essential for the Motor Inhibition

(A) A combined ribbon and stick-model representation showing the packing interface between CC1 and the β-finger in the CC1-FHA dimer structure. CC1 adopts an amphipathic helix, and the C-terminal half of CC1 forms a short coiled coil, which contacts with only one of the two β-fingers in the CC1-FHA dimer. The side chains of the residues involved in the interface packing are drawn in explicit atomic model.

(B) Biochemical characterization of the CC1/β-finger fragment. Both the analytical gel-filtration analysis (B1) and the sedimentation velocity-based assay (B2) showed that the CC1/β-finger fragment exists as a monomer in solution.

(C) Cellular localizations of the MD-NC-CC1-BF fragment and its various mutants. Compared to WT MD-NC-CC1-BF (C1), deletion of the CC1/β-finger region significantly increased the cell peripheral localizations (C2). In line with the inhibitory roles of CC1 and the β-finger, the MD-NC-CC1-BF fragments with various mutations in the C-terminal end of CC1 (C3) and the β-finger (C4–C5) showed much more prominent localizations at the cell periphery. The indistinct cell body is marked with an arrow. Scale bar: 20 μm.

(D) Quantification of the cellular distribution data showed in (C). The ratio of the tip to cell body average FI was quantified for each construct for more than 15 cells (n > 15). The error bars represent mean (±SD), ***p < 0.001.

See also Figures S3 and S5.

(L469Q/M472Q) largely restored the cell peripheral localizations (Figures 4C3 and 4D). More interestingly, either deletion of the β-finger ([474-486]Δ) or mutation of the hydrophobic residues in the β-finger (V474N) all highly increased the cell peripheral localizations of MD-NC-CC1-BF, demonstrating that the β-finger also plays an essential role in the motor inhibition (Figures 4C4, 4C5, and 4D). As expected, the dimeric forms of all the above CC1/β-finger mutants could be observed (Figure S5).

before the FHA domain, which included CC1 and the β-finger. Thus, we wondered whether CC1 and the β-finger are both essential for the motor inhibition. To test this, we first investigated the cellular localizations of the MD-NC-CC1-BF fragment of KIF1A (the same fragment used by Hammond et al., 2009) with various deletions or point mutations in the CC1/β-finger region (Figure 4C). Compared with the MD-NC-CC1-BF control (existing in a monomeric form and mainly localized in the cell body), deletion of both CC1 and the β-finger essentially restored the motor activity, and the remaining MD-NC fragment could be detected as a dimeric form and was largely localized at the cell periphery (Figures 4C1, 4C2, and 4D, and Figure S5). Consistent with the role of CC1 in the motor inhibition, mutations of the hydrophobic residues at the C-terminal end of CC1

Next, we asked whether the inhibitory roles of both CC1 and the β-finger may exist in the longer KIF1A fragment. Given that KIF1AΔCT (a KIF1A fragment without the C-terminal tail, i.e., MD-NC-CC1-FHA-CC2) has been demonstrated to be the minimum fragment with a similar motor behavior to the full-length protein (Hammond et al., 2009), we next checked both the cellular localizations and the microtubule binding capacities of KIF1AΔCT and its various mutants with the same set of mutations in the CC1/β-finger region. Consistent with the reported data, wild-type (WT) KIF1AΔCT showed somewhat even distributions from the cell body to the cell periphery without the obvious microtubule binding capacity (Figures 5A1, 5B, 6A1, and 6B). In contrast, KIF1AΔCT carrying the mutations in the CC1/β-finger region ([474-486]Δ, V474N, and L469Q/M472Q)

Structure

The CC1-FHA Tandem As a Motor Regulation Hub
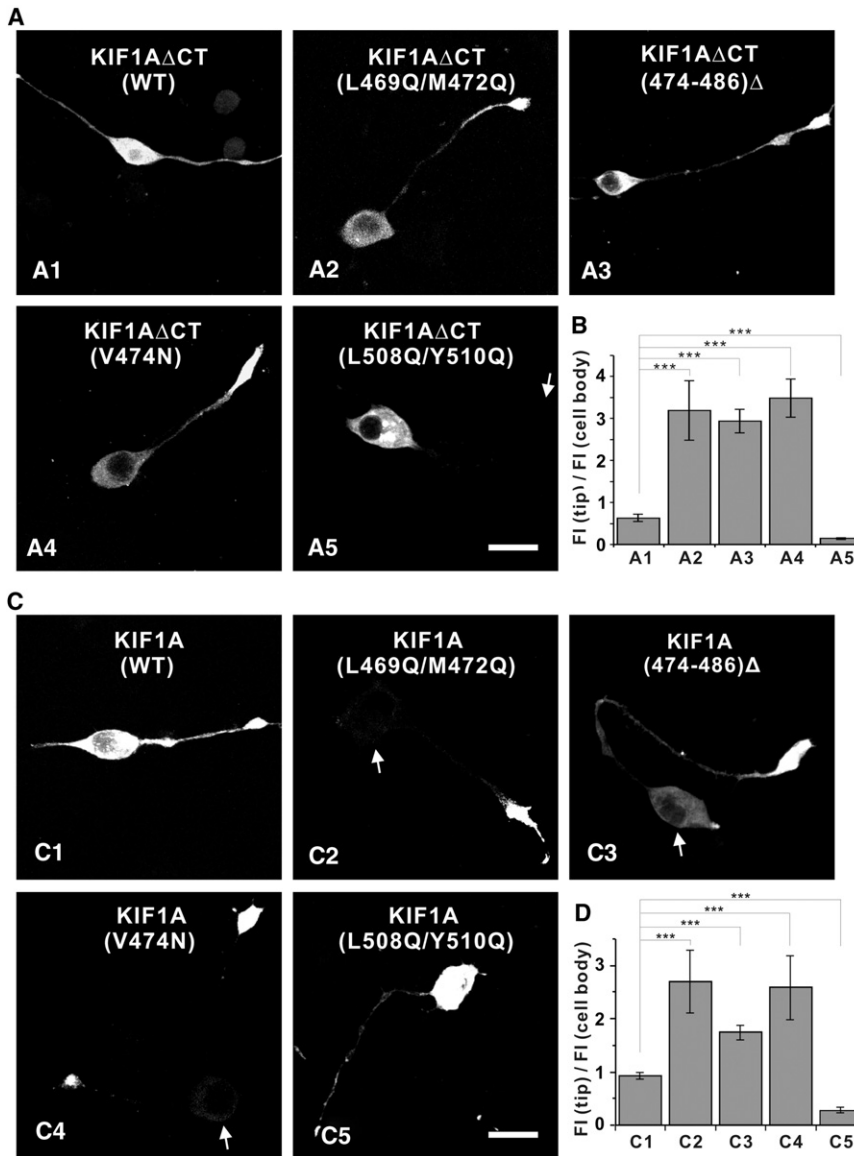
Figure 5. Dissociation of the CC1-FHA Dimer Regulates the Motor Activity

(A) Cellular localizations of KIF1AΔCT and its various mutants. Compared to WT-KIF1AΔCT (A1), those KIF1AΔCT constructs with mutations in the β-finger or in CC1 showed increased cell peripheral localizations (A2–A4), indicating the essential roles of the CC1/β-finger region in the motor inactivation. In contrast, KIF1AΔCT only with the mutations in the FHA domain, which causes the CC1-FHA dimer dissociation without any effects on the CC1/β-finger region, showed more prominent localizations in the cell body (A5). The indistinct cell tip is marked with an arrow. Scale bar: 20 μm.

(B) Quantification of the cellular distribution data showed in (A). The ratio of the tip to cell body average FI was quantified for each construct for more than 15 cells (n > 15). The error bars represent mean (±SD), ***p < 0.001.

(C) Cellular localizations of the full-length KIF1A and its various mutants. Compared to WT-KIF1A (C1), KIF1A with mutations in the β-finger or CC1 also showed increased cell peripheral localizations (C2–C4). In contrast, KIF1A with the mutations in the FHA domain was more prominently localized in the cell body (C5). The indistinct cell body is marked with an arrow. Scale bar: 20 μm.

(D) Quantification of the cellular distribution data showed in (C). The quantification method followed that for (B). The error bars represent mean (±SD), ***p < 0.001.

See also Figures S4 and S5.
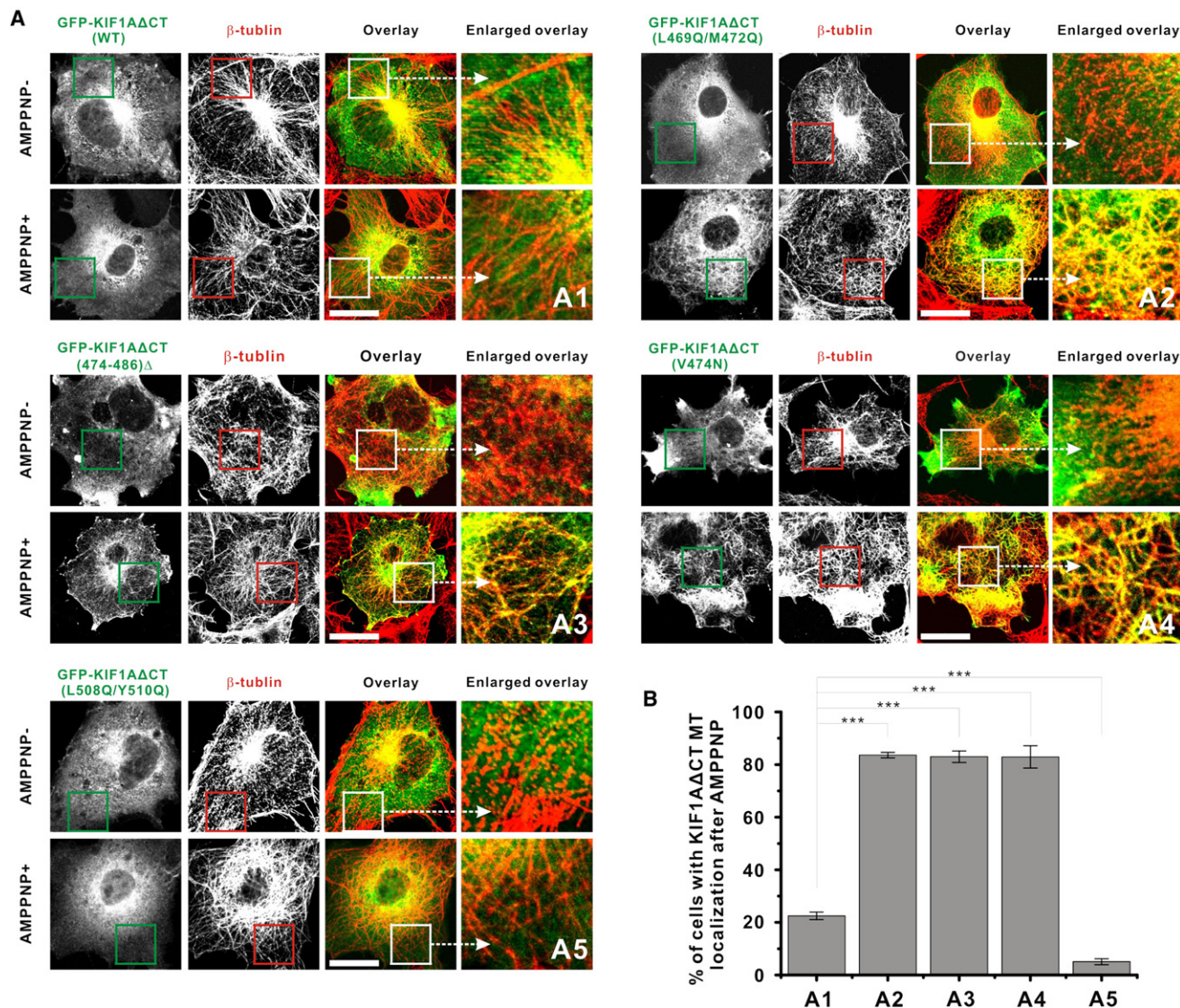
Dissociation of the CC1-FHA Dimer in KIF1A Inhibits the Motor Activity

We demonstrated above that the C-terminal half of CC1 and the β-finger are essential for the motor inactivation (Figures 4 and 5); however, both of them are directly involved in the formation of the CC1-FHA dimer (Figures 1 and 3). Thus, the CC1/β-finger region is unlikely to be available for the motor inhibition in the CC1-FHA dimer, and dissociation of the CC1-FHA dimer would conversely release the CC1/β-finger region for exerting its function. To test this hypothesis, we again first checked the cellular localizations and the microtubule binding capacities of KIF1AΔCT and its mutants carrying the mutations to dissociate the CC1-FHA dimer (Figures 5 and 6). As the CC1/β-finger region is essential for the motor inhibition, the mutations in CC1/β-finger region (such as [474-486]Δ, V474N, and L469Q/M472Q) not only disrupt the CC1-FHA dimer formation (Figure S2), but also concurrently impair the inhibitory capacity of this region (Figure S4). Thus, we had to pick up another couple of point mutations located in the FHA domain (L508Q/Y510Q), which can dissociate the CC1-FHA dimer but without any effects on either CC1 or the β-finger (Figures S2 and S4). Furthermore, the L508Q/Y510Q mutant was shown to stay in a monomeric state (Figure S5). Compared with the cellular distributions of WT

were all found to bind to microtubules and to be enriched at the cell periphery (Figures 5A2–A4, 5B, 6A2–6A4, and 6B), indicating that the inhibition of the motor was released by these mutations. Thus, the resulting KIF1AΔCT mutants are likely to be in their constitutively active forms, possibly due to the disruption of the CC1/β-finger-mediated inhibition of the NC dimerization (Figure S4). Furthermore, all these mutants were demonstrated to exist in dimeric conformations (Figure S5). To consolidate the above results, we checked the cellular localizations of the full-length KIF1A and its various mutants (with the same set of mutations in the CC1/β-finger region), which showed the similar dimeric state and cellular distribution profile to KIF1AΔCT and its mutants, respectively (Figures 5C and 5D and Figure S5), demonstrating that both CC1 and the β-finger play essential roles for the motor inhibition in the full-length protein.

Figure 6. Dissociation of the CC1-FHA Dimer Regulates the Microtubule-Binding Capacity of the Motor
(A) In vivo microtubule-binding assay of KIF1AΔCT and its various mutants. Compared to WT-KIF1AΔCT (A1), L508Q/Y510Q-KIF1AΔCT (A5) showed fewer microtubule binding/colocalization events, albeit none of them had obvious microtubule binding capacity with AMPPNP treated. In contrast, KIF1AΔCT with various mutations in the β-finger or in CC1 showed significant microtubule bindings/colocalizations after being treated with AMPPNP (A2–A4). Scale bar: 20 μm.
(B) Quantification of the in vivo microtubule-binding data showed in (A). The percentage of cells showing the microtubule colocalizations was quantified for each KIF1AΔCT construct (average of four experiments, n > 45 cells each). The error bars represent mean (±SD), ***p < 0.001.
See also Figure S5.

KIF1AΔCT, the L508Q/Y510Q-KIF1AΔCT showed more prominent localizations in cell body and fewer microtubule binding events (Figures 5A5, 5B, 6A5, and 6B), demonstrating that dissociation of the CC1-FHA dimer by the L508Q/Y510Q substitutions releases the CC1/β-finger region for the further inhibition of the motor activity. We also checked the cellular distributions of the full-length KIF1A with the L508Q/Y510Q mutations, which again showed the similar monomeric state and cellular distribution profile to the L508Q/Y510Q-KIF1AΔCT (Figures 5C and 5D and Figure S5), indicating that dissociation of the CC1-FHA dimer further inhibits the motor activity in the full-length KIF1A as well.

DISCUSSION

Kineisn-3 KIF1A Acts as a Processive Dimer
Due to the fact that kinesin-3 KIF1A adopts a globular monomer in vitro, the motor was defined as an unconventional kinesin (Okada et al., 1995). However, recent studies of KIF1A in vivo have demonstrated that the motor is able to form a processive dimer (Hammond et al., 2009). The NC-mediated dimerization of the motor is critical for its processive movement, although the NC dimer seems to be not very stable (Rashid et al., 2005; Tomishige et al., 2002). Here, we demonstrated that the CC1-FHA tandem (not separated CC1 or the FHA domain),

Structure

The CC1-FHA Tandem As a Motor Regulation Hub

immediately following MD-NC, forms a stable dimer in solution, thus implying that the central region of KIF1A may function similarly to that (the coiled-coil stalk) of the conventional kinesin kinesin-1 for promoting the motor dimer formation (Figure 1A). As such, KIF1A is likely to function as a processive dimer analogous to kinesin-1 motors. Further structural studies of the CC1-FHA dimer in this study may provide a bona fide explanation for the formation of an active KIF1A dimer (Figure 7). In this "two-headed" dimer working model, the NC dimer is largely responsible for bringing the two motor heads together. The CC1-FHA tandem located in the middle of the motor may act as an additional dimeric core for the assembly of the KIF1A dimer, which would synergistically function together with the NC dimer to control the motor's processive movement. The CC1-FHA tandem may also be able to dictate the motor dimerization by modulating the NC dimer formation (Figure 7 and Figure S5). It is likely that the C-terminal PH domains of the two KIF1A proteins may further facilitate the dimer formation by simultaneously binding to cargo vesicles (Klopfenstein et al., 2002) (Figure 7).

The CC1-FHA Tandem of KIF1A as a Motor Regulation Hub

The most unexpected feature of the CC1-FHA tandem is the β-finger structure formed by the covalent linker between CC1 and the FHA domain (Figures 1 and 3). Consistent with this feature, the cryo-EM studies of UNC-104 revealed that the CC1/FHA linker is not flexible but may form a well-folded structure (Al-Bassam et al., 2003). In the CC1-FHA structure, CC1 adopts a single amphipathic helix with a large tendency to form a bundle-like structure upon binding to its potential targets (Figures S1 and S3). In line with these characteristics, CC1 has been reported to sequester NC with the two domains packing in parallel and forming a bundle-like structure (Al-Bassam et al., 2003). In their model, the flexile hinge between NC and CC1 is also essential for the intramolecular NC/CC1 packing, and the C-terminal half of CC1 is largely responsible for the interaction with NC. We showed that the conserved hydrophobic residues in the C-terminal half of CC1 is essential for the motor inhibition (Figures 4 and 5), which may reflect the role of the C-terminal half of CC1 for the association with NC.

Both CC1 and the β-finger were demonstrated to be essential for the inhibition of the motor activity in KIF1AΔCT and the full-length KIF1A (Figure 5). Given that the CC1-FHA dimer is largely assembled by the C-terminal half of CC1, the β-finger, and part of the FHA domain (Figures 1 and 3), most parts of the C-terminal half of CC1 and the β-finger should be buried in the dimer interface and are unavailable for the motor inhibition. Thus, in addition to promoting the motor dimer formation, dimerizaiton of the CC1-FHA tandem would be able to activate the KIF1A motor by relieving the CC1/β-finger-mediated inhibition (Figure 7). The CC1-FHA tandem is likely to function as a motor regulation hub, and the monomer-dimer interconversion of the CC1-FHA tandem may also play a critical role in controlling the activation-inactivation of the motor (Figure 7). Amino acid sequence analysis of the CC1-FHA tandem of kinesin-3 motors revealed that the critical residues for the CC1-FHA dimer formation are highly conserved (Figure S6), suggesting that the CC1-FHA tandem-mediated dimerization and the resulting regulation
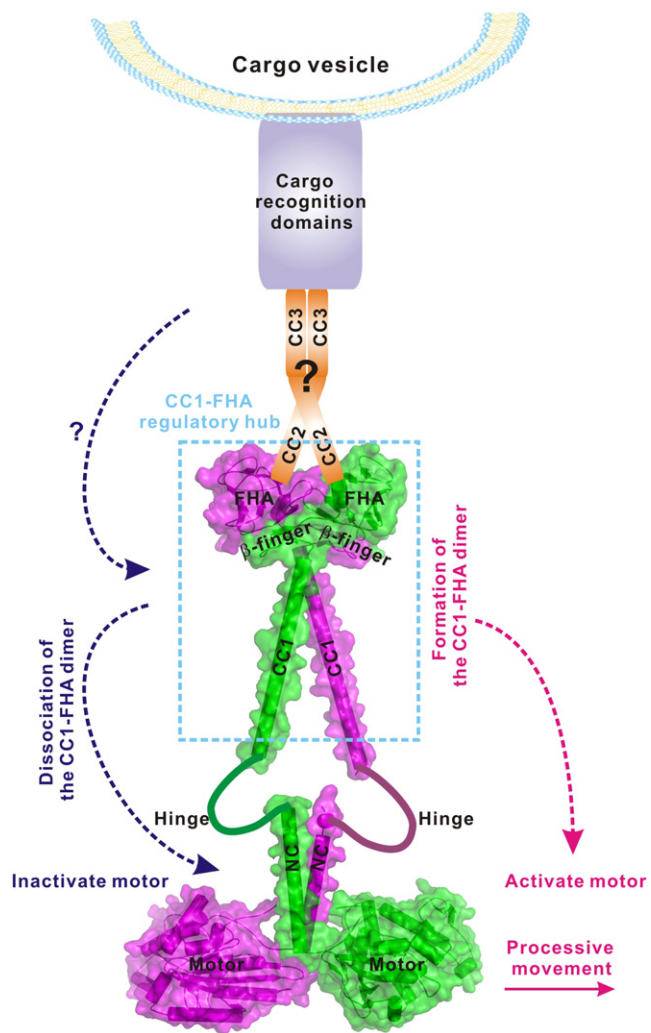
Figure 7. A Schematic Working Model Showing an Active, Processive KIF1A Dimer

In this drawing, both MC-NC (the same region of the conventional kinesin (PDB code: 3KIN) was used as the model) and the CC1-FHA tandem are drawn in a combined surface and ribbon representation, and for clarity, other regions of KIF1A are shown as simple cartoons. KIF1A is likely to form a processive dimer analogous to kinesin-1 motors. The NC-mediated dimerization is a critical step for the formation of a processive dimer, which is inhibited by the CC1/β-finger region (marked with the blue dashed arrow). Dimerization of the CC1-FHA tandem not only promotes the KIF1A dimer formation but also release the inhibition of NC by sequestering the CC1/β-finger region (marked with the red dashed arrow). CC2 immediately following the FHA domain can fold back and would likely regulate the motor activity by controlling the CC1-FHA dimer. Thus, the CC1-FHA tandem may function as a regulatory hub, and the monomer-dimer interconversion of the CC1-FHA tandem would control the motor activity (marked with the dashed box). It is unclear whether CC2 or CC3 could further enhance the motor dimerization. The C-terminal cargo-recognition domains (such as the PH domain) are responsible for binding to cargo adaptors/vesicles, which would further promote the clustering/dimerization of the motor. Given the critical role of the CC1-FHA tandem for the activation and dimerization of the motor, the regulation of the CC1-FHA dimer may represent a key step for controlling the motor's processive movement. Nevertheless, due to the current studies only focus on the CC1-FHA tandem, the working model presented here definitely needs to be further tested with the longer KIF1A fragments. See also Figure S6.

mechanism are also conserved features common to all members of kinesin-3 motors.

Dimerization of the CC1-FHA Tandem Could Be Regulated by CC2

In the CC1-FHA-CC2 cassette (Figure 1A), CC2 has been reported to interact with the FHA domain and adopt a folded-back conformation for inhibiting the motor activity. However, the molecular mechanism underlying the CC2-mediated regulation remains largely elusive, as there are no direct interactions between CC2 and MD-NC (Lee et al., 2004). In the C-CC1-FHA structure, the last helix (αC) of one FHA domain directly contacts with the $\beta1/\beta2$-loop of the other FHA domain (Figures 1C and 2E), which may stabilize the dimer formation. Since CC2 immediately follows the C-terminal end of αC, it would be possible that the direct packing of CC2 with the FHA domain has some impacts on the contacts between αC and the $\beta1/\beta2$-loop, thus leading to the destabilization of the CC1-FHA dimer. Consistent with this speculation, the full-length KIF1A was demonstrated to be a monomer in vitro (Okada et al., 1995), and the cryo-EM studies of UNC-104 showed that the MD-NC-CC1-FHA-CC2 fragment of the motor adopts a monomeric form (Al-Bassam et al., 2003). Given that dissociation of the CC1-FHA dimer would release the CC1/β-finger region for the motor inactivation, CC2 might play a critical role in the regulation of the CC1-FHA dimer as for the CC2-mediated inhibition (Figure S4).

WT full-length KIF1A and KIF1AΔCT (containing CC2) showed similar in vivo cellular profile with somewhat even distributions from the cell body to the cell periphery (Figure 5), indicating that both of these two KIF1A fragments may exist in a partial activation status, likely due to a mixture of monomeric and dimeric forms of the motor (e.g., in a dynamic monomer-dimer equilibrium mediated by CC2 at the high concentrations of the motor) (Figure S4). Supporting this speculation, KIF1A could be detected as a dimeric form in vivo, and dissociation of CC2 from the FHA domain significantly promoted the formation of the full-length KIF1A dimer (Hammond et al., 2009; Lee et al., 2004). Our cellular distribution data may further support the monomer-dimer equilibrium hypothesis, as the point mutations on the FHA domain that dissociates the CC1-FHA dimer further inhibited the motor activity (Figures 5 and 6), possibly due to switching all the dimeric motors to the monomeric forms. Thus, the potential CC2-mediated regulation of the CC1-FHA dimer may provide an explanation for the monomer-dimer transition of KIF1A from in vitro to in vivo.

The Motor Regulation Mechanism of KIF1A Might Be Exceptional

The negative regulatory region of kinesin-1 KIF5A is located at the extreme C-terminal tail. In contrast, the CC1-FHA-CC2 regulatory cassette of kinesin-3 KIF1A sits in the middle of the motor and closely follows MD-NC (Figure 1A), indicating that the regulation mechanism of the KIF1A motor might be distinct. In kinesin-1 motors, the C-terminal regulatory tail generally folds back to interact with MD-NC and lock the motor activity, which can be released by the tail-mediated cargo binding (Coy et al., 1999; Friedman and Vale, 1999; Verhey and Hammond, 2009). In kinesin-2 KIF17, a similar mechanism is likely to be employed by the motor to control the motor activity with its C-terminal

regulatory tail (Hammond et al., 2010; Verhey et al., 2011). However, in kinesin-3 KIF1A, CC1 in the central CC1-FHA-CC2 cassette is capable of sequestering NC directly, which prohibits the NC dimer formation (Al-Bassam et al., 2003; Hammond et al., 2009). More exquisitely, we found in this study that the CC1-mediated inhibition can be released by the formation of the CC1-FHA dimer, which would also concomitantly promote the NC-mediated dimerization of the motor (Figure 7). Therefore, the monomer-dimer conversion of the CC1-FHA tandem would likely have a "chain-reaction" effect on the dimerization and activation of KIF1A, which is somewhat different from the motor activation mechanism of other kinesin motors and may represent a new paradigm for the kinesin regulation.

EXPERIMENTAL PROCEDURES

Protein Expression and Purification

DNA sequences encoding human KIF1A fragments, including CC1-FHA (residues 430–607), C-CC1-FHA (residues 458–607), FHA (residues 480–607), and CC1 (residues 430–491), and various mutants were cloned into a modified version of the pET32a vector individually. Point mutations of KIF1A fragments were created using the standard PCR-based mutagenesis method and confirmed by DNA sequencing. Recombinant proteins were expressed in *Escherichia coli* BL21 (DE3) host cells at 16°C. The GB1-His$_6$-tagged fusion proteins were purified by Ni^{2+}-NTA agarose (QIAGEN) affinity chromatography followed by size-exclusion chromatography (Superdex-200, GE healthcare). After cleavage of the GB1-tag, the resulting proteins were further purified by another step of size-exclusion chromatography.

Crystallization, Data Collection, and Structure Determination

Crystals of CC1-FHA (10 mg/ml in 50 mM Tris-HCl, 100 mM NaCl [pH 7.5]) and C-CC1-FHA (10 mg/ml in 50 mM Tris-HCl, 100 mM NaCl [pH 8.0]) were obtained using the hanging-drop method by mixing 1 μl protein sample with equal volume of 18% (w/v) PEG 5000 MME, 8% (v/v) Tacsimate (pH 6.0) and 0.1 M Bis-Tris (pH 5.8) at 16°C, and 0.2 M calcium acetate hydrate, 18% (w/v) PEG 3000, 0.1 M Bis-Tris (pH 7.2) at 16°C, respectively. Crystals of CC1-FHA and C-CC1-FHA were cryoprotected in mother liquid supplemented with 15% (v/v) glycerol and 3% (v/v) glycerol, respectively, and then flash-frozen by plunging into liquid nitrogen. Diffraction data were collected at the Shanghai Synchrotron Radiation Facility (SSRF) BL17U with a wavelength of 0.979 Å at 100K, and processed and scaled using HKL2000 (Otwinowski and Minor, 1997).

Regarding the CC1-FHA structure determination, the FHA domain structure was solved by the molecular replacement method using the KIF13B FHA domain (PDB code: 3FM8) as the search model with PHASER (McCoy, 2007). Residues of CC1 were manually modeled into the structure according to the *2Fo-Fc* and *Fo-Fc* electron density maps, and residues or side chains lacking densities were not included in the model. The structure was further fitted and rebuilt with COOT (Emsley and Cowtan, 2004), and refined with REFMAC5 (Murshudov et al., 1997) and CNS (Brünger et al., 1998). At the final stage of refinement, TLS refinement was used with groups defined by the TLSMD server (Painter and Merritt, 2006). The overall quality of the final structural model was assessed by PROCHECK (Laskowski et al., 1993). For the C-CC1-FHA structure determination, the procedures were followed as those for the determination of the CC1-FHA structure, except that the CC1-FHA structure was used as the search model for the molecular replacement method.

Cell Culture, Imaging, and Data Analysis

Truncated KIF1A constructs MD-NC-CC1-BF (residues 1–491) and KIF1AΔCT (residues 1–771) were PCR amplified from the full-length KIF1A (Lee et al., 2003) and cloned into pEGFP-N1 vector. All mutants were produced by the standard PCR-based mutagenesis method. N2A cells were cultured in DMEM/F-12 (1:1) containing 10% fetal bovine serum. COS-7 and HEK293 cells were cultured in DMEM containing 10% fetal bovine serum. The cells were transfected by Lipofectamine 2000 (Invitrogen) or electroporation (Amaxa) according to the manufacturer's instructions.

Structure

The CC1-FHA Tandem As a Motor Regulation Hub

Fluorescence images were obtained on an Olympus FV500 laser scanning confocal microscope with 60× (NA = 1.40) oil objective. Confocal settings used for image capture were held constant in comparison experiments. The images were processed and analyzed by ImageJ (NIH). For the cellular distribution data analysis, the specific regions of the cell body (excluding the nucleus) and the tip of each cell were chosen, and the average fluorescence intensities (FI) were calculated, respectively. All the final quantification graphs were generated by EXCEL (Microsoft).

In Vivo Microtubule-Binding Assay

COS-7 cells were transfected with plasmids encoding the proteins of interest. At 48 hr posttransfection, the cells were treated with 0.05 unit/μl SLO (Sigma) in permeabilization buffer (PB; 25 mM HEPES/KOH, 115 mM potassium acetate, 5 mM sodium acetate, 5 mM MgCl2, 0.5 mM EGTA, and 10 mg/ml BSA [pH 7.4]), 2 mM AMPPNP (5′-adenylyl-beta,gamma-imidodiphosphate) (Sigma) and 10 μM taxol (Cytoskeleton) for 10 min (the equal amounts of PB buffer was substituted for control samples), and then fixed with 4% paraformaldehyde (Sigma). The fixed cells were permeablilized with PBS containing 0.1% Triton X-100, and blocked with 5% goat serum for 1 hr. After being washed three times with PBS, the cells were incubated with the special antibody (Protein STAR) to β-tubulin for 1 hr, the secondary antibody (CY3) (Jackson ImmunoResearch Laboratories, Inc.) for 1 hr and then imaged. For the microtubule-binding data analysis, if the KIF1A fragment formed fiber-like structures after being treated with AMPPNP and showed obvious colocalizations with the microtubules, the cell was counted as the one showing the microtubule-binding/colocalization event.

REFERENCES

Aizawa, H., Sekine, Y., Takemura, R., Zhang, Z., Nangaku, M., and Hirokawa, N. (1992). Kinesin family in murine central nervous system. J. Cell Biol. 119, 1287–1296.

Al-Bassam, J., Cui, Y., Klopfenstein, D., Carragher, B.O., Vale, R.D., and Milligan, R.A. (2003). Distinct conformations of the kinesin Unc104 neck regulate a monomer to dimer motor transition. J. Cell Biol. 163, 743–753.

Brünger, A.T., Adams, P.D., Clore, G.M., DeLano, W.L., Gros, P., Grosse-Kunstleve, R.W., Jiang, J.S., Kuszewski, J., Nilges, M., Pannu, N.S., et al. (1998). Crystallography & NMR system: a new software suite for macromolecular structure determination. Acta Crystallogr. D Biol. Crystallogr. 54, 905–921.

Coy, D.L., Hancock, W.O., Wagenbach, M., and Howard, J. (1999). Kinesin's tail domain is an inhibitory regulator of the motor domain. Nat. Cell Biol. 1, 288–292.

Emsley, P., and Cowtan, K. (2004). Coot: model-building tools for molecular graphics. Acta Crystallogr. D Biol. Crystallogr. 60, 2126–2132.

Erlich, Y., Edvardson, S., Hodges, E., Zenvirt, S., Thekkat, P., Shaag, A., Dor, T., Hannon, G.J., and Elpeleg, O. (2011). Exome sequencing and disease-network analysis of a single family implicate a mutation in KIF1A in hereditary spastic paraparesis. Genome Res. 21, 658–664.

Friedman, D.S., and Vale, R.D. (1999). Single-molecule analysis of kinesin motility reveals regulation by the cargo-binding tail domain. Nat. Cell Biol. 1, 293–297.

Gennerich, A., and Vale, R.D. (2009). Walking the walk: how kinesin and dynein coordinate their steps. Curr. Opin. Cell Biol. 21, 59–67.

Hammond, J.W., Cai, D., Blasius, T.L., Li, Z., Jiang, Y., Jih, G.T., Meyhofer, E., and Verhey, K.J. (2009). Mammalian Kinesin-3 motors are dimeric in vivo and move by processive motility upon release of autoinhibition. PLoS Biol. 7, e72.

Hammond, J.W., Blasius, T.L., Soppina, V., Cai, D., and Verhey, K.J. (2010). Autoinhibition of the kinesin-2 motor KIF17 via dual intramolecular mechanisms. J. Cell Biol. 189, 1013–1025.

Hirokawa, N., Noda, Y., Tanaka, Y., and Niwa, S. (2009). Kinesin superfamily motor proteins and intracellular transport. Nat. Rev. Mol. Cell Biol. 10, 682–696.

Huckaba, T.M., Gennerich, A., Wilhelm, J.E., Chishti, A.H., and Vale, R.D. (2011). Kinesin-73 is a processive motor that localizes to Rab5-containing organelles. J. Biol. Chem. 286, 7457–7467.

Klopfenstein, D.R., Tomishige, M., Stuurman, N., and Vale, R.D. (2002). Role of phosphatidylinositol(4,5)bisphosphate organization in membrane transport by the Unc104 kinesin motor. Cell 109, 347–358.

Laskowski, R.A., Macarthur, M.W., Moss, D.S., and Thornton, J.M. (1993). Procheck - a Program to Check the Stereochemical Quality of Protein Structures. J. Appl. Crystallogr. 26, 283–291.

Lawrence, C.J., Dawe, R.K., Christie, K.R., Cleveland, D.W., Dawson, S.C., Endow, S.A., Goldstein, L.S., Goodson, H.V., Hirokawa, N., Howard, J., et al. (2004). A standardized kinesin nomenclature. J. Cell Biol. 167, 19–22.

Lee, J.R., Shin, H., Choi, J., Ko, J., Kim, S., Lee, H.W., Kim, K., Rho, S.H., Lee, J.H., Song, H.E., et al. (2004). An intramolecular interaction between the FHA domain and a coiled coil negatively regulates the kinesin motor KIF1A. EMBO J. 23, 1506–1515.

Lee, J.R., Shin, H., Ko, J., Choi, J., Lee, H., and Kim, E. (2003). Characterization of the movement of the kinesin motor KIF1A in living cultured neurons. J. Biol. Chem. 278, 2624–2629.

Liang, X., and Van Doren, S.R. (2008). Mechanistic insights into phosphoprotein-binding FHA domains. Acc. Chem. Res. 41, 991–999.

Mahajan, A., Yuan, C., Lee, H., Chen, E.S., Wu, P.Y., and Tsai, M.D. (2008). Structure and function of the phosphothreonine-specific FHA domain. Sci. Signal. 1, re12.

McCoy, A.J. (2007). Solving structures of protein complexes by molecular replacement with Phaser. Acta Crystallogr. D Biol. Crystallogr. 63, 32–41.

Murshudov, G.N., Vagin, A.A., and Dodson, E.J. (1997). Refinement of macromolecular structures by the maximum-likelihood method. Acta Crystallogr. D Biol. Crystallogr. 53, 240–255.

Okada, Y., Yamazaki, H., Sekine-Aizawa, Y., and Hirokawa, N. (1995). The neuron-specific kinesin superfamily protein KIF1A is a unique monomeric motor for anterograde axonal transport of synaptic vesicle precursors. Cell 81, 769–780.

Otwinowski, Z., and Minor, W. (1997). Processing of X-ray diffraction data collected in oscillation mode. Macromolecular Crystallography. Pt A 276, 307–326.

Painter, J., and Merritt, E.A. (2006). TLSMD web server for the generation of multi-group TLS models. J. Appl. Crystallorg. *39*, 109–111.

Park, M., Watanabe, S., Poon, V.Y., Ou, C.Y., Jorgensen, E.M., and Shen, K. (2011). CYY-1/cyclin Y and CDK-5 differentially regulate synapse elimination and formation for rewiring neural circuits. Neuron *70*, 742–757.

Rashid, D.J., Bononi, J., Tripet, B.P., Hodges, R.S., and Pierce, D.W. (2005). Monomeric and dimeric states exhibited by the kinesin-related motor protein KIF1A. J. Pept. Res. *65*, 538–549.

Rivière, J.B., Ramalingam, S., Lavastre, V., Shekarabi, M., Holbert, S., Lafontaine, J., Srour, M., Merner, N., Rochefort, D., Hince, P., et al. (2011). KIF1A, an axonal transporter of synaptic vesicles, is mutated in hereditary sensory and autonomic neuropathy type 2. Am. J. Hum. Genet. *89*, 219–230.

Tomishige, M., Klopfenstein, D.R., and Vale, R.D. (2002). Conversion of Unc104/KIF1A kinesin into a processive motor after dimerization. Science *297*, 2263–2267.

Tsai, J.W., Lian, W.N., Kemal, S., Kriegstein, A.R., and Vallee, R.B. (2010). Kinesin 3 and cytoplasmic dynein mediate interkinetic nuclear migration in neural stem cells. Nat. Neurosci. *13*, 1463–1471.

Vale, R.D. (2003). The molecular motor toolbox for intracellular transport. Cell *112*, 467–480.

Verhey, K.J., and Hammond, J.W. (2009). Traffic control: regulation of kinesin motors. Nat. Rev. Mol. Cell Biol. *10*, 765–777.

Verhey, K.J., Kaul, N., and Soppina, V. (2011). Kinesin assembly and movement in cells. Annu. Rev. Biophys. *40*, 267–288.

Woehlke, G., and Schliwa, M. (2000). Walking on two heads: the many talents of kinesin. Nat. Rev. Mol. Cell Biol. *1*, 50–58.

Yildiz, A., and Selvin, P.R. (2005). Kinesin: walking, crawling or sliding along? Trends Cell Biol. *15*, 112–120.

Yonekawa, Y., Harada, A., Okada, Y., Funakoshi, T., Kanai, Y., Takei, Y., Terada, S., Noda, T., and Hirokawa, N. (1998). Defect in synaptic vesicle precursor transport and neuronal cell death in KIF1A motor protein-deficient mice. J. Cell Biol. *141*, 431–441.